Mid-infrared ultrafast carrier dynamics in thin film black phosphorus

2017 2D Mater. 4 021032

(http://iopscience.iop.org/2053-1583/4/2/021032)

2D Materials

RECEIVED
20 March 2017

REVISED
18 May 2017

ACCEPTED FOR PUBLICATION
22 May 2017

PUBLISHED
9 June 2017

LETTER

Mid-infrared ultrafast carrier dynamics in thin film black phosphorus

Vasudevan Iyer[1], **Peide Ye**[2] **and Xianfan Xu**[1]

[1] Department of Mechanical Engineering and Birck Nanotechnology Center, Purdue University, West Lafayette, IN 47907, United States of America

[2] Department of Electrical and Computer Engineering and Birck Nanotechnology Center, Purdue University, West Lafayette, IN 47907, United States of America

E-mail: xxu@ecn.purdue.edu

Keywords: black phosphorus, mid-infrared spectroscopy, carrier dynamics, ultrafast spectroscopy

Supplementary material for this article is available online

Abstract

Black phosphorus is emerging as a promising semiconductor for electronic and optoelectronic applications. To study fundamental carrier properties, we performed ultrafast femtosecond pump-probe spectroscopy on thin film black phosphorus mechanically exfoliated on a glass substrate. Carriers (electrons and holes) were excited to high energy levels and the process of carrier relaxation through phonon emission and recombination was probed. We used a wide range of probing wavelengths up to and across the band gap to study the evolution of the relaxation dynamics at different energy levels. Our experiments revealed a plethora of important physical phenomena. The fast relaxation time constants, associated with carrier-phonon scattering, steadily increase as the energy of the probe beam approaches the band gap energy, which was determined to be 0.31 eV, and the carrier recombination rate was obtained when the probe wavelength was tuned to match the band gap energy. The carrier-phonon scattering rates were found to be similar along the armchair and zigzag directions, therefore, the anisotropic carrier mobility reported in literature is mainly due to the difference in effective mass of carriers along different directions. The ultrafast spectroscopy data further revealed the oxidation induced surface charges. Our results highlight the importance of using the spectroscopy technique, in this case, in the mid-IR range, to uncover useful physical processes.

Since the last decade there has been an increasing interest in the study of 2D materials, especially graphene and transition metal dichalcogenides (TMDC) for fabricating many electronic and optoelectronic devices [1–11]. Black phosphorus has emerged as a recent material in this field and has shown promises with its direct bandgap, anisotropic electronic, optical, and thermal properties, and good device performance [12–19]. Black phosphorus has a direct bandgap in the bulk of around 0.35 eV and can become as large as 1.5 eV in the monolayer form according to first principles calculations, photoluminescence studies, and electrical measurements [12, 13, 20–23]. The direct bandgap is attractive for use in electronic devices such as solar cells [24, 25] and photodetectors [26–29]. Black phosphorus has also been successfully tested as a transistor channel material [30–32].

Given the vast interest in black phosphorus, it is important to investigate its properties at a fundamental level. Ultrafast optical spectroscopy is very useful in understanding carrier scattering, relaxation, and recombination processes. Many ultrafast studies have been carried out on graphene [33–39] and TMDC such as MoS_2 [40–43]. There have also been a few ultrafast optical studies on black phosphorus which have brought out the enhancement of anisotropic behavior after photoexcitation [44], provided upper bounds for mobility values through spatial scanning study [45], and highlighted the carrier decay process at long time scales which was attributed to carrier lifetime, i.e. recombination [46]. A recent article investigated the decay process of excited carriers at short time scales on liquid exfoliated black phosphorus nanosheets and determined the carrier-phonon scattering times at a few different probing energy levels corresponding to commonly encountered laser emission lines [47].

Most ultrafast pump-probe studies are performed with one excitation wavelength and one probe wavelength. On the other hand, probing a range of wavelengths or equivalently a range of energy states,

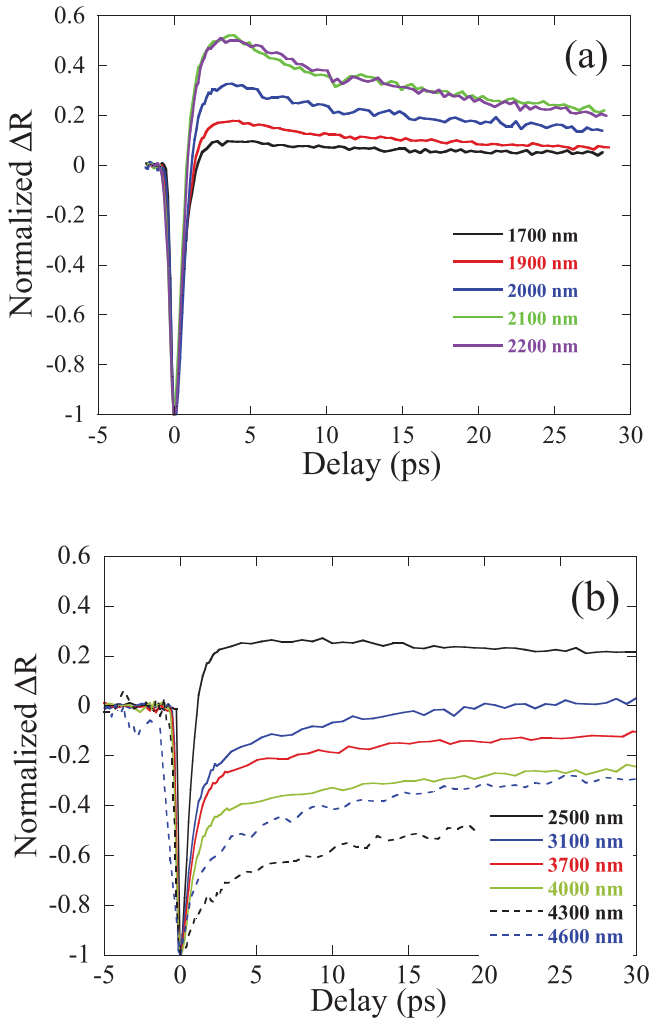

Figure 1. Transient reflectivity of black phosphorus for probing wavelengths from (a) 1700 nm to 2200 nm and (b) 2500 nm to 4600 nm.

especially near the band edge, can uncover the vital information about the carrier relaxation process as demonstrated for graphene and MoS_2 [33, 36, 48]. In this study, we focus on understanding the evolution of the decay of excited states with varied probe energy approaching the band gap of black phosphorus, and relate the ultrafast dynamics with fundamental transport properties. The scattering processes in black phosphorus in different directions are studied in order to gauge their importance in the observed anisotropic carrier mobility. A previous study [47] obtained a direction averaged scattering rate using randomly oriented flakes produced by liquid exfoliation and present the carrier dynamics at select probing energies. We systematically varied the probing direction and energies on a mechanically exfoliated flake, and find carrier scattering rates along the armchair and zigzag directions with a saturation of scattering time as the probe energy is tuned closer to and below the band edge, which helps to reveal the origin of anisotropic transport properties. The information on recombination was obtained when the probing wavelength was tuned to the band gap energy. Finally, the ultrafast spectroscopy data also revealed surface charge induced by oxidation.

The transient reflectance data obtained using the 792 nm pump wavelength polarized along the armchair direction and probe wavelengths varied from 1700 nm to 2200 nm, also polarized along the armchair direction are presented in figure 1(a). Data for wavelengths from 2500 nm to 4600 nm are shown in figure 1(b). All the datasets have been normalized by their minimum values to −1. Change in reflectance is defined as the reflectance after pump excitation minus the reflectance without any pump excitation. The details of the ultrafast experiment and flake exfoliation are provided in supplementary note 1 and 2 (stacks.iop.org/TDM/4/021032/mmedia), respectively.

During photoexcitation by a femtosecond laser pulse, carriers are generated at those energy levels in the conduction and valence band that correspond to vertical transitions in an E-k band diagram at the pumping energy. These carriers have momentum along the polarization direction of the pump. They then randomize their momentum and energy by carrier-carrier scattering processes. This randomization process is fast and beyond the measurement time resolution (see supplementary note 4). The next step is the formation of a thermalized distribution which can be represented by

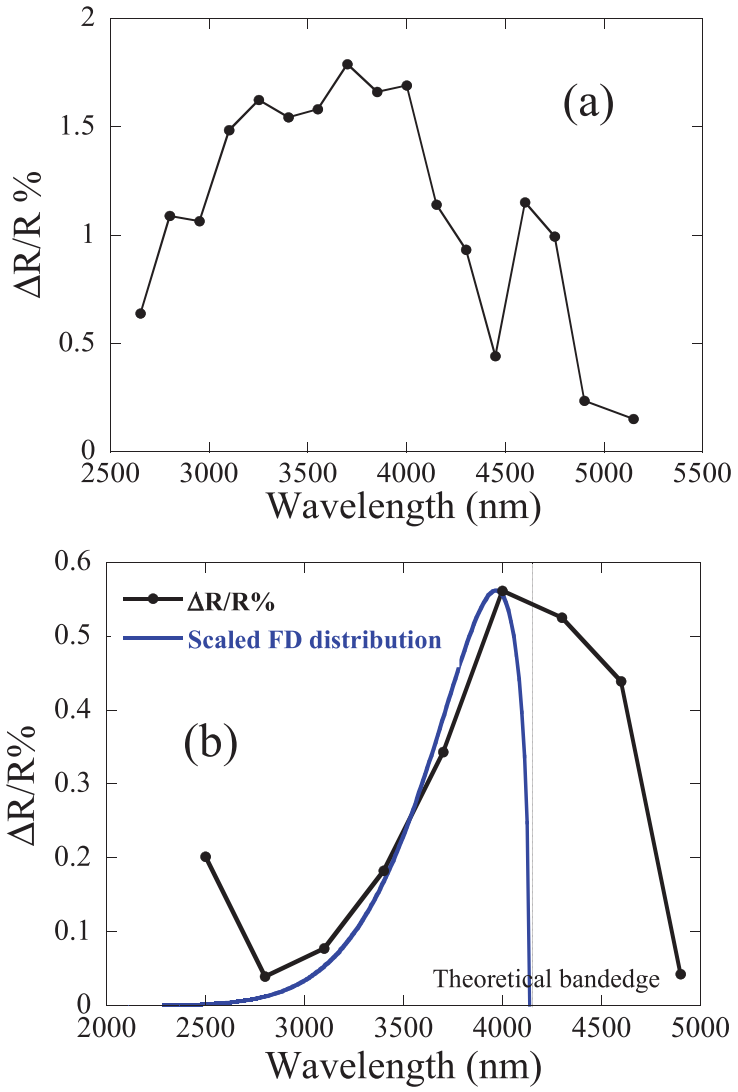

Figure 2. (a) $\Delta R(t=0)/R_0$ versus wavelength showing the bandgap near 0.31 eV and the presence of sub-band gap energy state. (b) $\Delta R(t=10\,\text{ps})/R_0$ showing the formation of Fermi–Dirac distribution.

the Fermi–Dirac (FD) distribution. In order to achieve thermalization, carriers must move closer to the band edge in energy space and this implies intraband relaxation. The first decay in the experimental data after the initial electron bleach (Pauli blocking), starting at zero picosecond (rising from $\Delta R = -1$) and of the order of one picosecond is attributed to carrier-phonon scattering leading to the formation of a thermalized carrier distribution [46, 47]. Pauli blocking is a result of occupation of carriers at the probing energy level. As the carriers emit phonons and relax to states closer to the band edge, the contribution from Pauli blocking diminishes, reflecting in the rise in the reflectivity signal. The second decay that starts from a few picoseconds, and is much slower, is attributed to the carrier recombination and lattice heating, and the time scales (10–100 ps) are in good agreement with published work [44–46]. This second decay is thus an interband relaxation process. As can be seen from figure 2(a), for wavelengths closer to the band edge, $\Delta R_{max}/R_0$ is greater. This is because energies closer to the band edge have a higher carrier population after carrier–carrier thermalization and thus produce a higher ΔR, though the distribution is non Fermi–Dirac. The data shown in figure 2(a) also indicates that the bulk bandgap is close to 4000 nm (0.31 eV), in agreement with previous theoretical work [12, 13, 20], recent FTIR data [49], and electrical measurements [23]. Additionally, a second peak about 40 meV below the band edge was also observed, which can be attributed to either exciton as theoretically predicted [20] or acceptor energy state as experimentally observed [50, 51]. Figure 2(b) shows $\Delta R/R_0$ at 10 ps delay time and a more Fermi–Dirac like behavior is evident by the comparison with the theoretically computed curve. The slight increase below 3000 nm is due to the sign change in the signal which arises due to the surface doping and will be discussed subsequently. Supplementary note 5 provides transmission data taken for a cluster of randomly oriented flakes. The band gap obtained from the transmission measurement fully agree with the ultrafast spectroscopy data presented in figure 2. The transient signal vanishes when the probe wavelength is above 4600 nm (below the sub-band gap energy state, supplementary note 6).

Bi-exponential fitting is used to extract the time constants for the fast and slow decays at different wavelengths:

$$\Delta R_{t>0} = A * \exp\left(-\frac{t}{\tau_1}\right) + B * \exp\left(-\frac{t}{\tau_2}\right) + C \quad (1)$$

The constant term C is attributed to the much slower thermal energy dissipation due to lattice heating. A and B are the amplitudes for the exponentials. τ_1 and τ_2 are the fast and slow decay times. Examples of fitting for the 2200 and 4000 nm probes using Equation (1) are shown in supplementary note 7, which show that the bi-exponential function can represent the signals well.

Figure 3(a) shows that the carrier-phonon scattering time at different energy levels approaches a value of about 1 ps as the probe energy approaches the band gap energy. This increase in the scattering time can be understood by the fact that as carriers approach the band edge, there are fewer channels to dissipate energy in the intraband relaxation process. From the Raman measurements, the optical phonon energy for black phosphorus is about 50 meV. Though there are other lower energy phonon modes, their strength (population) is much lower compared to the A_g and B_{2g} mode phonons [52]. Probing the sample with 0.4 eV (3100 nm) photons corresponds approximately to 50 meV above the band edge in both conduction and valence band. Since the excited carriers are expected to form a thermalized distribution a few meV above the band edge, carriers probed by 0.4 eV light are at the limit of one optical phonon emission, and probing with photon energy less than 0.4 eV leads to the relaxation time saturation behavior. Due to the femtosecond pulse width, the high bandwidth of the laser (20 meV energy resolution) is another limiting factor which could prevent us from observing the effects of lower energy phonon modes.

Using the carrier-phonon scattering times τ_1 obtained at the probing wavelength corresponding to the band gap, and $\mu = \frac{q\tau}{m^*}$, carrier mobility can be calculated. It is known that black phosphorus exhibits anisotropic transport properties along its armchair and zigzag directions such as mobility [12, 13]. Therefore, carrier-phonon scattering was also measured along the zigzag direction and is shown in the supplementary note 8. An ambipolar mobility of about 1900 $cm^2 V^{-1} \cdot s^{-1}$ along the zigzag direction and 22 000 $cm^2 V^{-1} \cdot s^{-1}$ along the armchair direction are obtained. The effective mass of electrons (holes) along the armchair direction is taken as 0.0825 (0.0761) m_0 whereas along the zigzag direction is 1.027 (0.648) m_0 [53]. Since electrons and holes have similar effective mass, the ambipolar mobility, defined as $\mu_a = \frac{2\mu_e\mu_h}{\mu_e + \mu_h}$, can be considered as an average carrier mobility. The ambipolar mobility is determined since the experimental data are a result of relaxation of both electrons and holes. The scattering time obtained is the upper limit for both holes and electrons, and given the comparable valence and conduction bands, similar scattering times are expected for electrons and holes. Our estimation of the mobility is reasonable compared to previous ultrafast experimental work (but with a probe wavelength of 810 nm) which determined a value of around 3000 $cm^2 V^{-1} \cdot s^{-1}$ for the zigzag direction and 50 000 $cm^2 V^{-1} \cdot s^{-1}$ for the armchair direction [45]. From figure 3 we can see the importance of probing near the bandgap to extract the correct scattering rates needed in calculations. Theoretical study predicted values in the 10^3 $cm^2 V^{-1} \cdot s^{-1}$ range [12]. However for fabricated devices, the mobilities were found not to exceed 1000 $cm^2 V^{-1} \cdot s^{-1}$ [13, 16, 30, 32, 54, 55]. The bulk and surface impurity scattering at equilibrium, which affects only the momentum of carriers (not their energy), would account for further reduction in mobility in devices which were not captured in the ultrafast spectroscopy experiments that are sensitive to changes in energy. Thus our experiment provides an upper limit for mobility.

The slow decay time (recombination time), τ_2, also increases when the probing wavelength approaches the band gap energy. This is because that the carriers, not at the band edge (4000 nm), scatter with phonons and move toward low energy levels. Hence, due to the additional relaxation channel, the higher energy carriers appear to have a faster recombination time. The recombination time, independent of carrier phonon scattering, must be evaluated at the bandgap energy. At the 4000 nm probing wavelength, the recombination time τ_2 is found to be about 18 ps. Figure 3(b) also shows that the recombination time at sub-band gap wavelength 4600 nm is about 12 ps. Since the data indicate both sub-band gap carriers and carriers in the delocalized bands relax with a comparable time, we expect a similar recombination mechanism for both, e.g. phonon assisted recombination. It is likely that the sub-band gap signal arises from acceptor states (versus from excitons) because it displays features similar to the band edge probe (4000 nm). These states are filled after rapid carrier–carrier scattering (fast drop in ΔR) and subsequently carrier-phonon scattering displaces carriers from the sub-band gap states to the delocalized states (fast rise in ΔR). For excitons, we would expect a different dynamics because the bound states should possibly show much longer decay times [48, 56].

It is worthwhile to look more closely at the relaxation process as the wavelength is varied. For shorter wavelengths (e.g. 2200 nm, figure 1(a)), a positive peak is observed, but the peak does not rise above zero for wavelengths longer than 3100 nm (figure 1(b)). We propose that such optical response is related to surface charges. It is known that oxidation can induce surface doping on the order of 10^{12} cm^{-2} [32]. Photoexcited holes in the bulk thermalize close to the band edge whereas photoexcited holes at the surface thermalize with the existing hole population due to doping by oxidation (see supplementary note 9). This creates an excess hole population at slightly higher energies in the valence

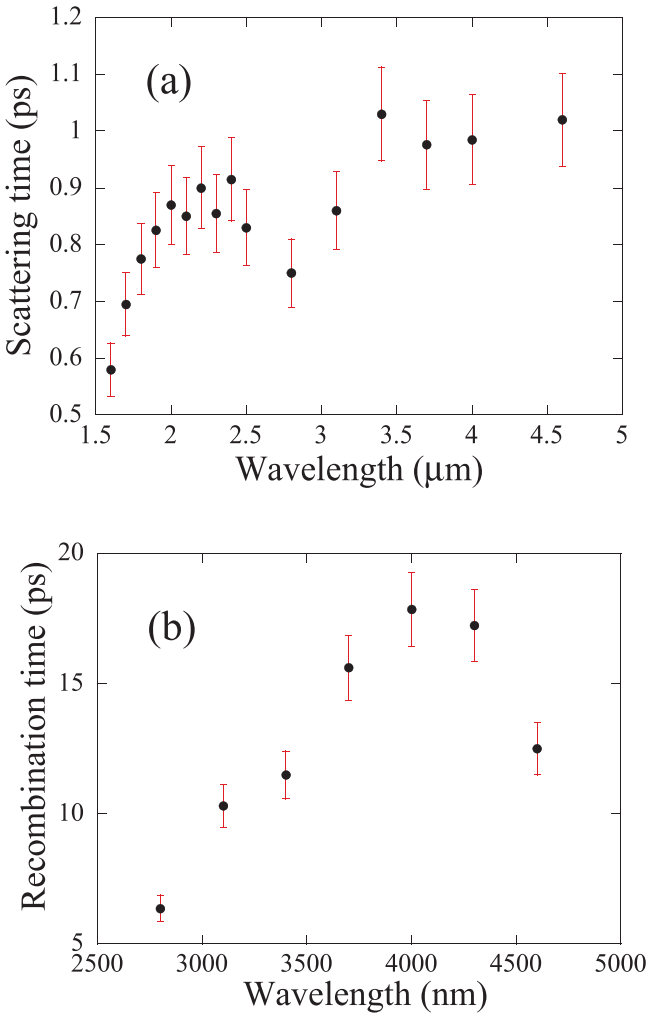

Figure 3. (a) Fast and (b) slow time constants with different probe energy. The fit uncertainty is about 8%.

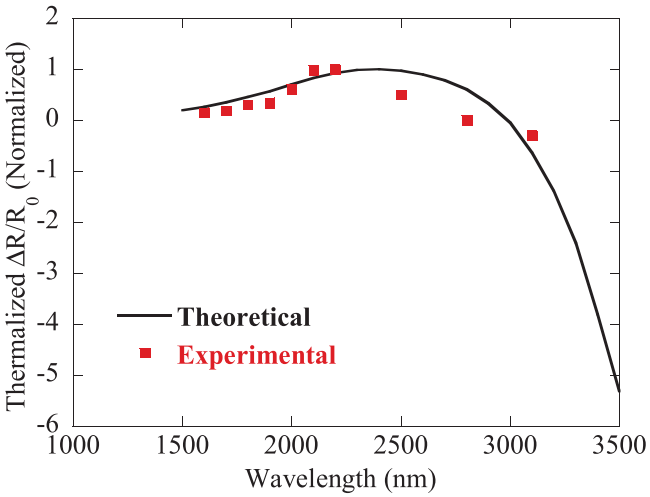

Figure 4. Theoretical estimate of $\Delta R/R$ and experimental values around 2000 nm. The experimental points are at 3 ps delay, i.e. after thermalization.

band and changes the dielectric constant. The change in dielectric constant is reflected in the spectroscopy data, which indicates variation of the (peak) reflectivity at different probing wavelengths corresponding to different energy levels in the valence band. We performed a calculation of the change in the dielectric constant at the surface and bulk and related it to the change in reflectivity in supplementary note 9. Results of the calculated reflectivity reproduces the observed positive change in reflectivity signals, as shown in figure 4.

In conclusion, we have carried out ultrafast infrared spectroscopy on thin film black phosphorus and found that the near band gap phonon-scattering time is close to 1 picosecond which is limited by the optical phonon scattering processes. By investigating energy relaxation of carriers with a tunable probe energy, it is found that carrier-phonon scattering time saturates when the probe energy reaches close to the band edge, which can be used to extract fundamental properties such as mobility. From the transient reflectivity data for different excitation and probing polarizations corresponding to the different anisotropic directions in black phosphorus, we find a similar scattering time along the armchair and zigzag directions. The major factor controlling the carrier mobility is thus the difference in the effective mass resulted from anisotropic band structure of the material rather than the scattering processes. The recombination time was also seen to increase as the probing wavelength approached the band edge. A sub-band gap energy state was also observed and attributed to acceptor states. Lastly, we used an optical property model for qualitatively explaining the spectroscopic features in the data, and found contributions due to surface doping by oxidation. Our work shows the importance of selecting the right probing wavelengths to study carrier dynamics in semiconductors displaying variety of interesting phenomena.

Acknowledgments

The authors would like to thank Anurup Dutta for his help with the atomic force microscope measurement and Prabhu Kumar for dielectric constant measurement. This work was supported by AFOSR/NSF under EFRI 2-DARE Grant EFMA-1433459.

The authors declare no competing financial interests.

References

[1] Butler S *et al* 2013 Progress, challenges, and opportunities in two-dimensional materials beyond graphene *ACS Nano* **7** 2898–926
[2] Eda G and Maier S 2013 Two-dimensional crystals: managing light for optoelectronics *ACS Nano* **7** 5660–5
[3] Wang Q, Kalantar-Zadeh K, Kis A, Coleman J and Strano M 2012 Electronics and optoelectronics of two-dimensional transition metal dichalcogenides *Nat. Nanotechnol.* **7** 699–712
[4] Ganatra R and Zhang Q 2014 Few-layer MoS_2: a promising layered semiconductor *ACS Nano* **8** 4074–99
[5] Bao Q and Loh K 2012 Graphene photonics, plasmonics, and broadband optoelectronic devices *ACS Nano* **6** 3677–94
[6] Jariwala D, Sangwan V, Lauhon L, Marks T and Hersam M 2014 Emerging device applications for semiconducting two-dimensional transition metal dichalcogenides *ACS Nano* **8** 1102–20
[7] Radisavljevic B, Radenovic A, Brivio J, Giacometti V and Kis A 2011 Single-layer MoS_2 transistors *Nat. Nanotechnol.* **6** 147–50
[8] Xu M, Liang T, Shi M and Chen H 2013 Graphene-like two-dimensional materials *Chem. Rev.* **113** 3766–98
[9] Avouris P 2010 Graphene: electronic and photonic properties and devices *Nano Lett.* **10** 4285–94
[10] Fiori G, Bonaccorso F, Iannaccone G, Palacios T, Neumaier D, Seabaugh A, Banerjee S and Colombo L 2014 Electronics based on two-dimensional materials *Nat. Nanotechnol.* **9** 768–79
[11] Liu M, Yin X, Ulin-Avila E, Geng B, Zentgraf T, Ju L, Wang F and Zhang X 2011 A graphene-based broadband optical modulator *Nature* **474** 64–7
[12] Qiao J, Kong X, Hu Z, Yang F and Ji W 2014 High-mobility transport anisotropy and linear dichroism in few-layer black phosphorus *Nat. Commun.* **5** 4475
[13] Liu H, Neal A, Zhu Z, Luo Z, Xu X, Tomanek D and Ye P 2014 Phosphorene: an unexplored 2D semiconductor with a high hole mobility *ACS Nano* **8** 4033–41
[14] Low T, Rodin A, Carvalho A, Jiang Y, Wang H, Xia F and Neto A 2014 Tunable optical properties of multilayer black phosphorus thin films *Phys. Rev.* B **90** 075434
[15] Castellanos-Gomez A 2015 Black phosphorus: narrow gap, wide applications *J. Phys. Chem. Lett.* **6** 4280–91
[16] Xia F, Wang H and Jia Y 2014 Rediscovering black phosphorus as an anisotropic layered material for optoelectronics and electronics *Nat. Commun.* **5** 4458
[17] Deng Y, Luo Z, Conrad N, Liu H, Gong Y, Najmaei S, Ajayan P, Lou J, Xu X and Ye P 2014 Black phosphorus-monolayer MoS_2 van der waals heterojunction p-n diode *ACS Nano* **8** 8292–9
[18] Luo Z, Maassen J, Deng Y, Du Y, Garrelts R, Lundstrom M, Ye P and Xu X 2015 Anisotropic in-plane thermal conductivity observed in few-layer black phosphorus *Nat. Commun.* **6** 8572
[19] Lee S *et al* 2015 Anisotropic in-plane thermal conductivity of black phosphorus nanoribbons at temperatures higher than 100 K *Nat. Commun.* **6** 8573
[20] Tran V, Soklaski R, Liang Y and Yang L 2014 Layer-controlled band gap and anisotropic excitons in few-layer black phosphorus *Phys. Rev.* B **89** 235319
[21] Wang X, Jones A, Seyler K, Tran V, Jia Y, Zhao H, Wang H, Yang L, Xu X and Xia F 2015 Highly anisotropic and robust excitons in monolayer black phosphorus *Nat. Nanotechnol.* **10** 517–21
[22] Zhang S *et al* 2014 Extraordinary photoluminescence and strong temperature/angle-dependent Raman responses in few-layer phosphorene *ACS Nano* **8** 9590–6
[23] Keyes R 1953 The electrical properties of black phosphorus *Phys. Rev.* **92** 580–4
[24] Buscema M, Groenendijk D, Steele G, van der Zant H and Castellanos-Gomez A 2014 Photovoltaic effect in few-layer black phosphorus PN junctions defined by local electrostatic gating *Nat. Commun.* **5** 4651
[25] Bai L, Sun L, Wang Y, Liu Z, Gao Q, Xiang H, Xie H and Zhao Y 2017 Solution-processed black phosphorus/pcbm hybrid heterojunctions for solar cells *J. Mater. Chem.* A **5** 8280–6
[26] Guo Q *et al* 2016 Black phosphorus mid-infrared photodetectors with high gain *Nano Lett.* **16** 4648–55
[27] Engel M, Steiner M and Avouris P 2014 Black phosphorus photodetector for multispectral, high-resolution imaging *Nano Lett.* **14** 6414–7
[28] Youngblood N, Chen C, Koester S and Li M 2015 Waveguide-integrated black phosphorus photodetector with high responsivity and low dark current *Nat. Photon.* **9** 247–52
[29] Suess R, Leong E, Garrett J, Zhou T, Salem R, Munday J, Murphy T and Mittendorff M 2016 Mid-infrared time-resolved photoconduction in black phosphorus *2D Mater.* **3** 041006
[30] Li L, Yu Y, Ye G, Ge Q, Ou X, Wu H, Feng D, Chen X and Zhang Y 2014 Black phosphorus field-effect transistors *Nat. Nanotechnol.* **9** 372–7
[31] Li L, Engel M, Farmer D, Han S and Wong H 2016 High-performance p-type black phosphorus transistor with scandium contact *ACS Nano* **10** 4672–7
[32] Du Y, Yang L, Zhou H and Ye P 2016 Performance enhancement of black phosphorus field-effect transistors by chemical doping *IEEE Electron Device Lett.* **37** 429–32
[33] Winnerl S *et al* 2011 Carrier relaxation in epitaxial graphene photoexcited near the dirac point *Phys. Rev. Lett.* **107** 237401
[34] Carbone F, Aubock G, Cannizzo A, Van Mourik F, Nair R, Geim A, Novoselov K and Chergui M 2011 Femtosecond carrier dynamics in bulk graphite and graphene paper *Chem. Phys. Lett.* **504** 37–40

[35] Dawlaty J, Shivaraman S, Chandrashekhar M, Rana F and Spencer M 2008 Measurement of ultrafast carrier dynamics in epitaxial graphene *Appl. Phys. Lett.* **92** 042116
[36] Shang J, Yu T, Lin J and Gurzadyan G 2011 Ultrafast electron-optical phonon scattering and quasiparticle lifetime in cvd-grown graphene *ACS Nano* **5** 3278–83
[37] Breusing M, Kuehn S, Winzer T, Malic E, Milde F, Severin N, Rabe J, Ropers C, Knorr A and Elsaesser T 2011 Ultrafast nonequilibrium carrier dynamics in a single graphene layer *Phys. Rev.* B **83** 153410
[38] Wang H *et al* 2010 Ultrafast relaxation dynamics of hot optical phonons in graphene *Appl. Phys. Lett.* **96** 081917
[39] Huang L, Gao B, Hartland G, Kelly M and Xing H 2011 Ultrafast relaxation of hot optical phonons in monolayer and multilayer graphene on different substrates *Surf. Sci.* **605** 1657–61
[40] Mannebach E *et al* 2014 Ultrafast electronic and structural response of monolayer MoS_2 under intense photoexcitation conditions *ACS Nano* **8** 10734–42
[41] Nie Z, Long R, Sun L, Huang C, Zhang J, Xiong Q, Hewak D, Shen Z, Prezhdo O and Loh Z 2014 Ultrafast carrier thermalization and cooling dynamics in few-layer MoS_2 *ACS Nano* **8** 10931–40
[42] Strait J, Nene P and Rana F 2014 High intrinsic mobility and ultrafast carrier dynamics in multilayer metal-dichalcogenide MoS_2 *Phys. Rev.* B **90** 245402
[43] Wang H, Zhang C and Rana F 2015 Ultrafast dynamics of defect-assisted electron–hole recombination in monolayer MoS_2 *Nano Lett.* **15** 339–45
[44] Ge S *et al* 2015 Dynamical evolution of anisotropic response in black phosphorus under ultrafast photoexcitation *Nano Lett.* **15** 4650–6
[45] He J, He D, Wang Y, Cui Q, Bellus M, Chiu H and Zhao H 2015 Exceptional and anisotropic transport properties of photocarriers in black phosphorus *ACS Nano* **9** 6436–42
[46] Suess R, Jadidi M, Murphy T and Mittendorff M 2015 Carrier dynamics and transient photobleaching in thin layers of black phosphorus *Appl. Phys. Lett.* **107** 081103
[47] Wang K, Szydlowska B, Wang G, Zhang X, Wang J, Magan J, Zhang L, Coleman J, Wang J and Blau W 2016 Ultrafast nonlinear excitation dynamics of black phosphorus nanosheets from visible to mid-infrared *ACS Nano* **10** 6923–32
[48] Shi H, Yan R, Bertolazzi S, Brivio J, Gao B, Kis A, Jena D, Xing H and Huang L 2013 Exciton dynamics in suspended mono layer and few-layer MoS_2 2d crystals *ACS Nano* **7** 1072–80
[49] Zhang G, Huang S, Chaves A, Song C, Ozcelik V, Low T and Yan H 2017 Infrared fingerprints of few-layer black phosphorus *Nat. Commun.* **8** 14071
[50] Baba M, Izumida F, Takeda Y, Shibata K, Morita A, Koike Y and Fukase T 1991 Two-dimensional anderson localization in black phosphorus crystals prepared by bismuth-flux method *J. Phys. Soc. Japan* **60** 3777–83
[51] Akahama Y, Endo S and Narita S 1986 Electrical-properties of single-crystal black phosphorus under pressure *Physica* B + C **139** 397–400
[52] Sugai S and Shirotani I 1985 Raman and infrared reflection spectroscopy in black phosphorus *Solid State Commun.* **53** 753–5
[53] Narita S, Terada S, Mori S, Muro K, Akahama Y and Endo S 1983 Far-infrared cyclotron-resonance absorptions in black phosphorus single-crystals *J. Phys. Soc. Japan* **52** 3544–53
[54] Du Y, Neal A, Zhou H and Ye P 2016 Transport studies in 2D transition metal dichalcogenides and black phosphorus *J. Phys.: Condens. Matter* **28** 263002
[55] Liu H, Du Y, Deng Y and Ye P 2015 Semiconducting black phosphorus: synthesis, transport properties and electronic applications *Chem. Soc. Rev.* **44** 2732–43
[56] Kumar N, He J, He D, Wang Y and Zhao H 2013 Charge carrier dynamics in bulk MoS_2 crystal studied by transient absorption microscopy *J. Appl. Phys.* **113** 133702